Tailor-Made Asymmetric PVDF Hollow Fibers for Soluble Gas Removal

K. Li, J. F. Kong, Dongliang Wang, and W. K. Teo
Dept. of Chemical and Environmental Engineering, National University of Singapore, Singapore 119260

Tailor-made polyvinylidene fluoride (PVDF) asymmetric hollow-fiber membranes and their membrane modules were employed for soluble gas removal, such as H_2S from waste gas streams. This study focused on the techniques of fabricating and characterizing the PVDF asymmetric hollow-fiber membranes and their membrane modules for removal of H_2S using an aqueous solution containing 10% NaOH. A laminar parabolic velocity profile was used to characterize the flow of the H_2S gas mixture in the hollow-fiber lumen. Effects of operating conditions and the morphological structures of the membranes on the membrane's coefficient, k_{AM}, were examined both theoretically and experimentally. The capabilities of the hollow-fiber membranes developed for removal of H_2S from waste gas streams were evaluated and compared with conventional symmetric hydrophobic hollow-fiber membranes, such as polypropylene. An analysis of H_2S transfer across the more developed PVDF membranes reveals that the membrane's coefficient, k_{AM}, evaluated from its structure parameters, such as the effective surface porosity and mean radius, agreed well with the experimental data obtained from absorption experiments.

Introduction

Microporous hollow-fiber membranes employed in gas absorption or stripping processes have attracted considerable attention since the early 1980s. The membranes used act as a fixed interface and keep the gas and liquid phases separated while the mass transfer of gases takes place through the membrane. Depending on the membrane material, the physicochemical properties of the absorbing liquid, and the operating pressures employed, the pores of the membranes can be filled with either gas or liquid, which will result in large differences in the mass-transfer resistance of the membrane employed (Karoor and Sirkar, 1993; Kreulen et al., 1993a).

Microporous hollow-fiber membranes employed for gas absorption or stripping provide several advantages compared to conventional absorption or stripping processes such as bubble columns and packed beds. These include a larger interfacial area per unit volume, independent control of gas and liquid flow rates without any flooding, loading, or foaming, and a known gas–liquid interfacial area. Recognition of these advantages is reflected by the number of investigations on the use of membrane modules for gas absorption and stripping reported in the literature, including those by Zhang and Cussler (1985a,b), Yang and Cussler (1986), Cooney and Jackson (1989), Ahmed and Semmens (1992), Kreulen et al. (1993b,c), Costello et al. (1993), and Li et al. (1994). In most studies, however, emphasis was focused on the nonwetted-operating mode whereby the membrane pores are filled with gases. The primary reason for such an operating mode is quite obvious. Since the usual physical absorption processes used in industries are limited by the mass-transfer rates in the liquid phase, the overall mass-transfer coefficients in these cases are between 10^{-5} and 10^{-4} m/s (Danckwerts, 1970). Adding the mass-transfer resistance of the nonwetted membrane, which is several orders of magnitude smaller than that of liquid, results in a negligible effect on the overall mass-transfer coefficient. Due to the considerably larger interfacial area, the overall mass transfer per unit volume, $K_l a$, for the membrane module is therefore much higher than that of conventional columns. Thus, the membrane-based gas absorption or stripping offers a promising alternative.

The usefulness of microporous hydrophobic hollow-fiber membranes for gas-film-controlled systems such as NH_3 in

Correspondence concerning this article should be addressed to K. Li.

H_2SO_4, SO_2 in NaOH, and H_2S (low concentration) in NaOH is dependent on the magnitudes of the membrane resistance. As studied by Zhang and Cussler (1985b), the K_{AG} values measured in polypropylene hollow-fiber modules are in the 0.0035 to 0.0073-m/s range, which is considerably lower than the 0.01–0.1-m/s K_{AG} values measured in the conventional gas absorbers (Westerterp et al., 1984). Therefore, it is not surprising that the membrane resistance controls the absorption of all these gases in the membrane modules used by Zhang and Cussler (1985b). Although the high interfacial area per unit volume of hollow-fiber geometry may compensate for the reduced overall mass-transfer coefficient, further reduction of the membrane resistance, $1/k_{AM}$, may still be the key factor to improve the mass-transfer efficiencies for the gas-film-controlled systems. Li et al. (1998) studied the removal of H_2S from a gas mixture using a concentrated alkaline solution in an asymmetric polysulfone hollow-fiber membrane module. The experimentally evaluated membrane's coefficient, k_{AM}, for the polysulfone is in the 0.0125 to 0.025-m/s range, which is better than the value of 0.0073 obtained from symmetric microporous polypropylene membranes (Zhang and Cussler, 1985b). In addition, using the hollow-fiber membranes, that is, small cylindrical tubes, with the H_2S gas mixture flowing in it, the possible maldistribution may be reduced to a minimum. Thus, such membrane modules may be particularly suited for purification purposes such as the removal of a trace amount of H_2S from contaminant streams.

In this article, the mass transfer of H_2S across PVDF asymmetric hollow-fiber membranes was investigated experimentally. The membranes with different morphological structures were prepared and characterized, and the effects of operating conditions and the morphological structures on the membrane's coefficient, k_{AM}, were studied extensively. An aqueous solution containing 10% NaOH was used as the absorbent. Experimental data obtained from the absorption experiments were analyzed and compared with the structural parameters of the PVDF membranes that were developed. Finally, the capabilities of these hollow-fiber membranes for removing H_2S were evaluated and compared with conventional symmetric hydrophobic hollow-fiber membranes such as polypropylene.

Experimental Work

Preparation of hollow-fiber membranes

Commercially available polyvinylidene fluoride Kynar k-760 or k-720 (Elf Autochem, USA) was used as membrane material, and *N,N*-dimethylacetamide (DMAc) (Synthesis Grade, Merck) was used to prepare the polymer solution. Polyvinylpyrrolidone (PVP, K120) (GAF ISP Technologies, Inc. $M_w = 2{,}900{,}000$) was used as an additive. The effect of ethanol in both internal and external coagulation fluids on the membrane morphology was studied and the ethanol composition in water was varied between 0 and 100% (v/v).

The required quantity of DMAc was taken in a one-liter wide-neck reaction flask, and the PVDF chips were slowly added for 30 min. A Heidolph RZR 2000 stirrer was used at a low speed ($\sim$ 200 rpm) in the initial stage to make sure that each polymer chip wetted thoroughly to avoid the formation of polymer lumps during the later stages. After 20 min, the stirrer speed was increased to $\sim$ 300 rpm and the dope temperature was slowly raised from 22°C to 60°C by heating it in a silicone oil bath. The dope temperature was maintained constant at about 60°C until all the polymer chips were dissolved in the solvent. As polymer viscosity was increased, the stirring continued at a high speed ($\sim$ 500 rpm) for 5 h to ensure the complete dissolution of the polymer into DMAc. PVP as an additive was then added to the dope when required. The stirring was continued at room temperature until the PVP was completely dissolved. Finally, the polymer solution was degassed at room temperature.

The degassed PVDF dope was transferred to a stainless-steel reservoir and pressurized to 20–30 psig (138–207 kPa) using nitrogen. A tube-in-orifice spinneret was used to obtain hollow-fiber membranes. Water or ethanol or a mixture of the two was used as both the internal and external coagulants. Finally, the forming hollow fibers were passed through a water bath to complete the solidification process and thoroughly washed in water. Nine batches of the PVDF hollow fibers were made. Details of the spinning apparatus and the hollow-fiber spinning procedure can be found elsewhere (Deshmukh and Li, 1998), and the spinning conditions for these nine batches of hollow fibers are contained in Table 1.

Characterization of the hollow-fiber membranes

Before the absorption study, the hollow-fiber membranes that were prepared were characterized using scanning electron microscopy (SEM) and gas permeation techniques.

Scanning Electron Microscopy. The PVDF membranes prepared by the methods just described were examined using a scanning electron microscope (Hitachi Model S 4100). First, the hollow-fiber membrane was immersed in liquid nitrogen. After about 10 min, the frozen fiber was slowly flexed in the

Table 1. Hollow-Fiber Spinning Conditions and the Resulting Membrane's Average Pore Size and Effective Surface Porosity

Batch No.	Polymer Kynar	Dope Composition (PVDF/PVP/DMAc) (v/v%)	Internal Coagulant (Water/Ethanol) (v/v%)	External Coagulant (Water/Ethanol) (v/v%)	Average Pore Radius, r (μm)	Effective Surface Porosity, ϵ/L_p m^{-1}
1	k-760	20/0/80	100/0	100/0	0.0441	31.79
2	k-760	20/0/80	100/0	85/15	0.0324	18.77
3	k-760	20/0/80	100/0	50/50	0.0449	7.77
4	k-760	20/8/72	100/0	100/0	0.0229	1406.70
5	k-760	20/8/72	100/0	85/15	0.0399	1026.07
6	k-760	20/8/72	100/0	70/30	0.0512	820.44
7	k-720	22/8/70	100/0	100/0	0.0708	1554.52
8	k-720	22/8/70	50/50	100/0	0.0697	2833.16
9	k-720	22/8/70	0/100	100/0	0.1184	6978.87

Table 2. Geometric Characteristic of Hollow-Fiber Modules and Their Membrane Coefficient, k_{AM}, Obtained by Different Methods

Module (Batch) No.	No. of Fibers	Effective Length (m)	Fiber OD (mm)	Fiber ID (mm)	k_{AM}, m/s (Gas Permeation)	k_{AM}, m/s (Gas Adsorption)
1	30	0.105	0.760	0.440	2.36×10^{-4}	2.25×10^{-4}
2	30	0.120	0.650	0.397	1.15×10^{-4}	1.61×10^{-4}
3	30	0.120	0.675	0.375	5.84×10^{-5}	2.35×10^{-4}
4	11	0.120	0.888	0.469	6.78×10^{-3}	7.06×10^{-3}
5	30	0.120	0.884	0.431	7.19×10^{-3}	7.81×10^{-3}
6	30	0.120	0.884	0.385	6.64×10^{-3}	1.18×10^{-2}
7	30	0.135	0.750	0.425	1.48×10^{-2}	1.84×10^{-2}
8	20	0.120	1.063	0.625	2.69×10^{-2}	4.09×10^{-2}
9	20	0.120	1.063	0.625	8.21×10^{-2}	7.20×10^{-2}

liquid nitrogen and a clear cross-sectional fracture appeared. The fiber was then positioned on a metal holder and gold coated using a sputter coating operated under a vacuum. The SEM cross-sectional pictures of the fibers were taken at various magnifications.

Average Pore Size and Effective Surface Porosity. The average pore size and the effective surface porosity of the hollow-fiber membranes were obtained using the gas permeation method. Gas permeability, J_i, for a porous medium shows a pressure dependency and can be expressed as

$$J_i = \frac{2}{3}\left(\frac{8RT}{\pi M}\right)^{0.5}\frac{1}{RT}\frac{r\epsilon}{L_p} + \frac{\bar{p}}{8\mu RT}\frac{r^2\epsilon}{L_p},$$

or

$$J_i = K_0 + P_0\bar{p}. \tag{1}$$

A detailed derivation of Eq. 1 is given in the Appendix. Pure N_2 gas was selected as the standard gas for the permeation experiments, and the permeation flux through the prepared asymmetric hollow-fiber membranes was measured at different pressures. Details of the permeation experiments can be found elsewhere (Wang et al., 1995). By plotting the J_i with mean pressures according to Eq. 1, the average pore size can be calculated from the intercept (K_0) and slope (P_0):

$$r = \frac{16}{3}\left(\frac{P_0}{K_0}\right)\left(\frac{8RT}{\pi M}\right)^{0.5}\mu. \tag{2}$$

The effective surface porosity, ϵ/L_p also can be obtained from the slope as follows:

$$\frac{\epsilon}{L_p} = \frac{8\mu RTP_0}{r^2}. \tag{3}$$

The average pore size, r, and the effective calculated surface porosity, ϵ/L_p, are also given in Table 1.

Preparation of the hollow-fiber modules

The hollow-fiber modules designed for the experimental studies consisted of a 20-mm-diameter brass tube acting as a shell with equal ''tees'' at each end of the tube. Both tees were then connected to a reducer on which the fibers were sealed. The desired number of fibers, assembled as a bundle, was first pulled through the reducer, and then a liquid epoxy resin (fast setting type) was poured into the reducer to position the fibers. When the fast setting epoxy resin had set, a slow setting epoxy resin was also poured into the reducer, so that the gaps between the fibers and the internal surface of the reducer were filled. After the epoxy resin was completely cured, the same operation was repeated at the other end of the module. A total of nine hollow-fiber modules were fabricated from the hollow fibers prepared as just described. The geometric characteristics of the modules and the fibers are given in Table 2.

Experimental apparatus and procedure for absorption

The experimental setup for absorption of H_2S is presented in Figure 1. The feed gas mixture containing 1200 ppm H_2S in balance with N_2 was introduced into the fiber lumen at the desired flow rate. The inlet gas flow rate was controlled by a mass flow controller (5850E series, Brooks), while the outlet gas flow rate was monitored using a mass-flow sensor (5860E series, Brooks). An aqueous solution containing the 10% NaOH used as the absorbing liquid was introduced into the shell side of the hollow-fiber modules, where it was in countercurrent contact with the feed gas. The flow rate of the liquid absorbent was controlled by a rotameter (Tokyo Keiso). The pressure at the gas phase side was varied between 0 and 250 kPa (gauge), while that of the liquid side (usually higher than that at the gas phase side) was maintained at a level where no bubbles were formed in the liquid.

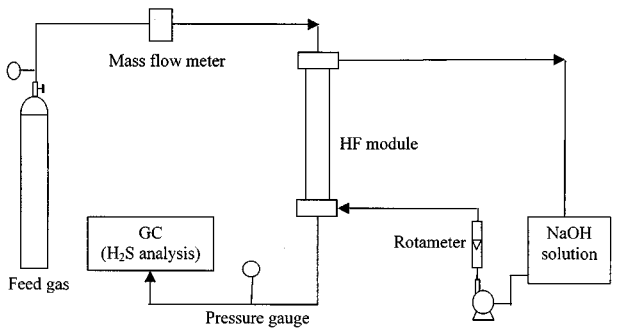

Figure 1. Experimental setup for H_2S absorption.

The compositions of the gas mixture in the outlet flow stream were determined by a Perkin-Elmer (Autosystem) gas chromatograph using a flame photometric detector (FPD). The detector response was recorded and analyzed by a personal computer with an ''Omega'' integration package developed by Perkin-Elmer. At each operating condition, four samples were taken at room temperature (25 ± 1°C), and the average value was calculated. The largest deviation between the samples and the average value is less than 6%. Finally, the average value, which represents the H_2S concentration in the outlet stream, was used to calculate the membrane's coefficient, k_{AM}.

Theory

Theoretical models have been derived to analyze the asymmetric hollow-fiber membrane's coefficient, k_{AM}. A gas mixture containing H_2S was continually fed into the fiber lumen, while a concentrated aqueous solution was introduced into the shell side. The following assumptions were utilized for the model development:

1. The reaction between the soluble gas and the reagent is instantaneous, and hence the concentration of the H_2S gas at the membrane–liquid interface is negligible.
2. There is a fully developed laminar flow in the tube side.
3. There is negligible axial dispersion in the tube side.
4. Tube- and shell-side pressures are constant.
5. The system is operated isothermally and at steady state.

Assumption 1 approximates the system realistically, so long as the reagent concentration in the liquid is high enough. Assumption 2 is valid for a Reynolds number that does not exceed 2100, which is true due to the very small diameter of the fibers. The entrance effect of the flow profile in the fiber lumen was ignored because it is not significant compared to the length of fiber used. Assumption 3 is viable, since the flow velocity in the tube side can be generally expected to be greater than the axial diffusion. Based on the preceding assumptions, the steady-state material-balance equations for the H_2S transfer across the lumen are given as follows:

$$U\frac{\partial C_a}{\partial z} = D_a\left(\frac{\partial^2 C_a}{\partial r^2} + \frac{1}{r}\frac{\partial C_a}{\partial r}\right)$$

$$2U_m\left[1-\left(\frac{r}{R}\right)^2\right]\frac{\partial C_a}{\partial z} = D_a\left(\frac{\partial^2 C_a}{\partial r^2} + \frac{1}{r}\frac{\partial C_a}{\partial r}\right), \qquad (4)$$

with boundary conditions

$$C_a|_{z=0} = C_{af} \qquad (0 \le r \le R) \qquad (5a)$$

$$\left.\frac{\partial C_a}{\partial r}\right|_{r=0} = 0 \qquad (0 \le z \le L). \qquad (5b)$$

Mass transfer of the H_2S across the membrane can be written as

$$D_a\left(\frac{\partial C_a}{\partial r}\right)_{r=R} = -k_{AM}(C_{aR} - C_{ai}). \qquad (5c)$$

The concentration of the H_2S gas at the membrane–liquid interface is assumed to be zero:

$$C_a|_{r=R_0} = C_{ai} = 0 \qquad (0 \le z \le L). \qquad (5d)$$

The ''mixing cup'' outlet concentration, $C_{a,\text{out}}$, is determined based on the following formula (Skelland, 1974a):

$$C_{a,\text{out}} = \frac{\int_0^R 2\pi\, rUC_a\, dr}{\int_0^R 2\pi\, rU\, dr}. \qquad (6)$$

We can see that Eqs. 4 to 6 correlate the H_2S concentration in the outlet stream, $C_{a,\text{out}}$, with the module characteristics and the operating conditions. With a known outlet concentration, $C_{a,\text{out}}$, the membrane's coefficient, k_{AM}, can be obtained using preceding derived equations.

The system of Eqs. 4 to 6 includes a partial differential equation of first-order and second-order. Solution of these equations to obtain k_{AM} has been attempted using orthogonal collocation techniques (Finlayson, 1971), the details are given elsewhere (Malek et al., 1997).

Results and Discussion

Morphology of PVDF hollow fibers

Nine PVDF hollow-fiber membranes were spun from polymer dopes with or without the PVP additive. The addition of the PVP was thought to be useful in obtaining porous membranes. A study on flat-sheet sulphonated PVDF membranes by Munari et al. (1990) showed that the PVP acts as a good pore-forming additive. The phase inversion technique with the addition of ethanol was used in either internal or external coagulants (water) in order to control the location of the skin in the formed PVDF hollow-fiber membranes.

Table 1 shows the average pore size and the effective surface porosity of the nine membranes obtained from the gas permeation analysis. The results reveal that addition of PVP has a negligible effect on the mean membrane pore size, but causes a drastic increase (two orders of magnitude) in the effective surface porosity. Considering that the PVP in the polymer dopes acts as an organic pore-former, the increase in the number of pores is expected.

The gas permeation method for determining the pore size and the effective surface porosity (open-end pores) was originally developed for symmetric membranes. For composite membranes with the different layers structured similarly, the mean measured pore size represents an overall contribution, while for an asymmetric membrane with a skin, the mean pore size may be regarded as a characteristic of the skin (Shih et al., 1990). As indicated by Shih et al., the mean pore size of the asymmetric membranes measured by the gas permeation method only represents a parameter that can be compared quantitatively with the membranes prepared under different spinning conditions. The mean pore size data in Table 1 suggest that the pores of the prepared PVDF membranes may be located in the skin wall, as the structural change in the substrate resulting from the presence of ethanol in either the external or internal coagulants has an insignificant effect on the mean pore size of the prepared membranes. The skin

of the membrane may be located in either the inner or outer skin wall, depending on the properties of the internal and external coagulants used. Determining the skin location in an asymmetric membrane can be more explicitly illustrated using the SEM, and this is presented below.

SEM micrographs of three typical coagulation conditions of the spun hollow-fiber membranes are shown in Figure 2. It can be seen that the skin location is largely dependent on the coagulation medium. The appearance of the fiber structure, that is, of both the inner and outer skins as shown in Figure 2a, can be attributed to the rapid precipitation that occurred at both the inner and the outer fiber walls, because water, a strong nonsolvent, is used as both the internal and external coagulants. When a substantial amount of ethanol was added to the external water coagulation bath, the rate of precipitation in the outer wall was greatly reduced, resulting in the elimination of the external skin, as shown in Figure 2b. Similarly, a considerable reduction in the precipitation rate in the inner wall by using ethanol as the internal coagulant, resulting in the internal skin of the PVDF hollow-fiber membrane being completely removed, as shown in Figure 2c. By retaining only one of the skins in the hollow-fiber membrane, the effective surface porosity, ϵ/L_p, may therefore be increased. As shown in Table 1, however, this is only true for membrane 9. For membranes 3 and 6, the opposite trends were observed. This contrary result is caused by the other factors simultaneously affecting the effective surface porosity, that is, the slow precipitation eliminates the asymmetric skin (decrease in L_p), while it may also increase the formation of dead pores (decrease of ϵ). These two opposite effects would either increase or decrease the effective surface porosity, ϵ/L_p, depending on which one is the dominating factor.

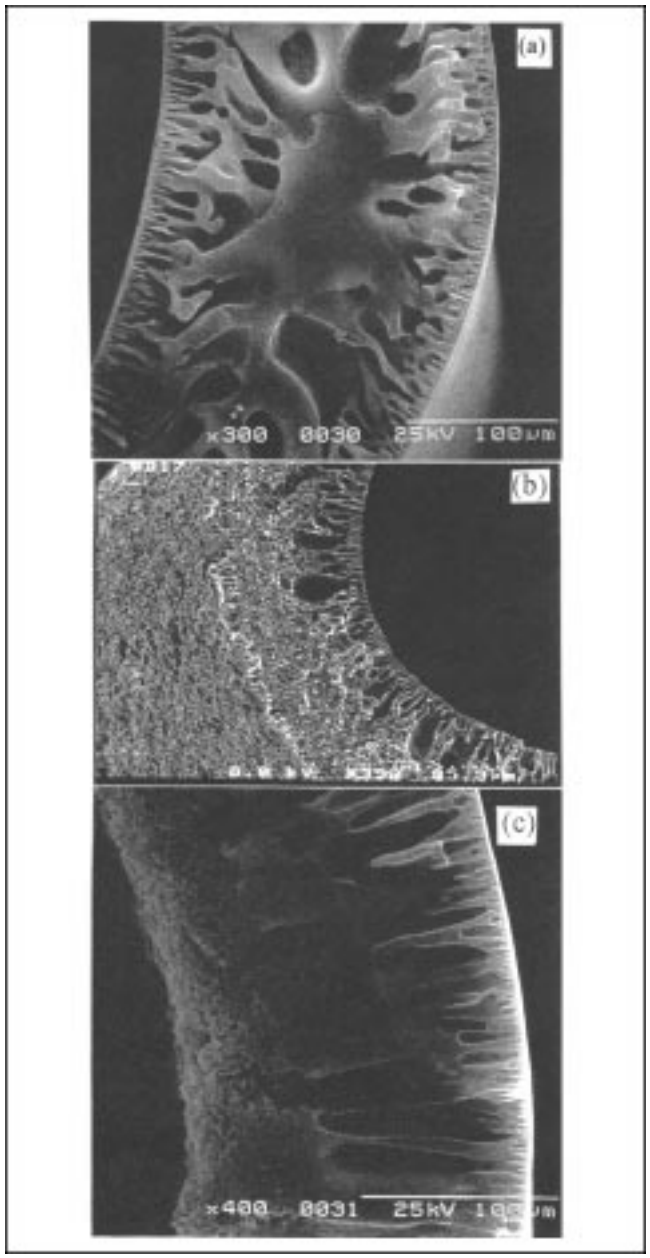

Figure 2. SEM micrographs of hollow-fiber membrane cross-section structures.

Hollow fibers were coagulated in (a) internal water, external water; (b) internal water, external 50:50 of ethanol:water; (c) internal ethanol, external water.

Membrane's coefficient, k_{AM}

Figures 3 and 4 show the H_2S depletion, $X_{a,\text{out}}$, defined as a ratio of the product concentration and the feed concentration of H_2S, $C_{a,\text{out}}/C_{af}$, as a function of the gas velocity in the hollow-fiber lumen for nine different modules. Table 1 shows that modules 1 to 3 were fabricated from the PVDF hollow fibers prepared from the polymer solutions with no PVP, while modules 4 to 9 contain fibers spun from the polymer solutions with PVP. Based on the SEM studies in the preceding subsection, the asymmetric skin for modules 4–6 is located in the inner fiber wall, while for modules 7 to 9, it is located in the outer wall. The H_2S depletion for modules 1 to 9 is plotted in Figure 3, where the symbols and solid lines represent the experimental data (obtained from the absorption experiments) and the calculated results, respectively. As can be seen from Figure 3a, module 9 provides a higher mass-transfer coefficient compared to modules 7 and 8. This is because the hollow fibers used for module 9 have no internal skin, which gives a lower mass transfer resistance for H_2S transfer. Similar trends can also be observed in Figures 3b and 3c. However, the effect is much less significant.

Figure 4 shows the effect of PVP on H_2S depletion, based on the results obtained from modules 3, 6, and 9. We can see that under the same operating conditions, the H_2S depletion achieved in modules 6 and 9 (with PVP) is much better than that achieved in module 3 (without PVP). The calculated results indicate that the membrane resistance, $1/k_{AM}$, for module 3 is almost two orders of magnitude higher than that for modules 6 and 9. As mentioned earlier, PVP is a good organic pore-former, so an increase in the effective porosity of the membranes can be expected after the PVP is added to the polymer solutions. With the much higher effective porosity of the membranes leading to a higher mass-transfer coefficient, k_{AM}, better H_2S depletion is expected under the same operation conditions.

For a nonwetted microporous membrane, that is, the pores are gas filled, the membrane's coefficient, k_{AM}, can also be

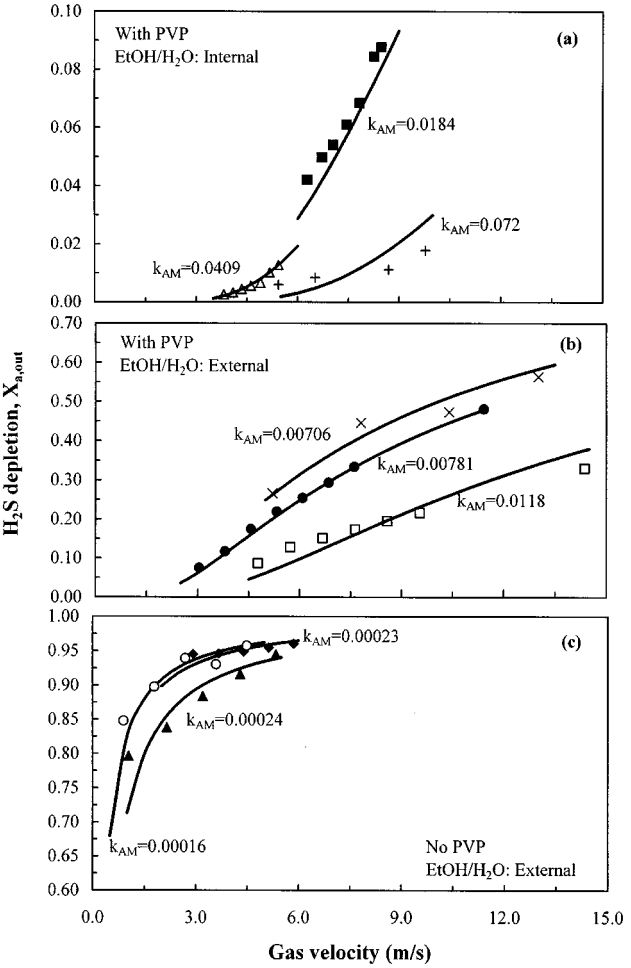

Figure 3. Experimental and calculated results for H_2S removal, obtained from nine modules: ○: 1; ♦: 2; ▲: 3; ×: 4; ●: 5; □: 6; ■: 7; △: 8; +: 9.

independently evaluated using their pore-structures property (Zhang and Cussler, 1985b; Kreulen et al., 1993a):

$$k_{AM} = \frac{D_{A,e}\epsilon}{\delta\tau_M}$$

or

$$k_{AM} = \frac{D_{A,e}\epsilon}{L_p}, \tag{7}$$

where ϵ and δ are the porosity and the thickness of the membrane, respectively; τ_M is the tortuosity, which corrects the membrane pore geometry; L_p is the effective thickness of the membrane, that is, $L_p = \delta\tau_M$. In Eq. 7, $D_{A,e}$ is the diffusion coefficient of the H_2S in membrane's gas-filled pores governed by both the continuum and the Knudsen diffusion coefficients, and is expressed by

$$\frac{1}{D_{A,e}} = \frac{1}{D_a} + \frac{1}{D_{AK}}. \tag{8}$$

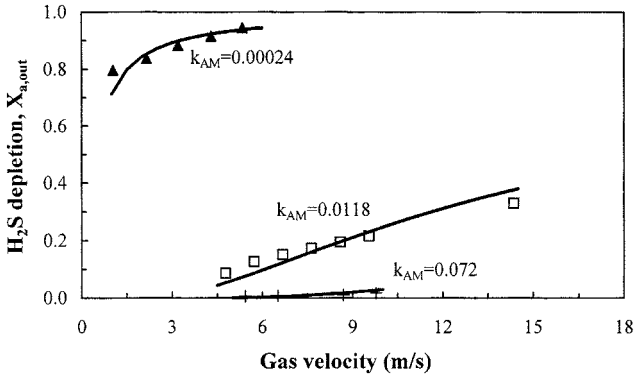

Figure 4. Effect of PVP and coagulant on H_2S depletion, experimental and calculated results obtained from membrane modules: ▲: 3; □: 6; +: 9.

In Eq. 8, D_{AK} is the Knudsen diffusion coefficient, and is expressed as

$$D_{AK} = \frac{2r}{3}\sqrt{\frac{8RT}{\pi M}}. \tag{9}$$

Based on Eqs. 7 to 9, the effect of pore radius on the membrane's transfer coefficient, k_{AM}, can be evaluated for different effective porosities, and is illustrated in Figure 5. It can be seen that as the pore radius is greater than 1 μm, the Knudsen diffusion effect becomes negligible and the membrane's transfer coefficient is governed only by the continuum diffusion coefficient. For the membranes prepared in this study, the average pore radius is considerably smaller than 1 μm (Table 1). Therefore, Eq. 8 is important in evaluating the diffusion coefficient of H_2S in the membrane pores.

With the gas permeation data given in Table 1, that is, the average pore radius and effective surface porosity, the membrane's coefficient, k_{AM}, was also evaluated using Eq. 7. The values of the membrane's coefficient obtained from Eq. 7 are compared in Table 2 with those obtained from the absorption experiments. It can be seen that for the same membrane, the

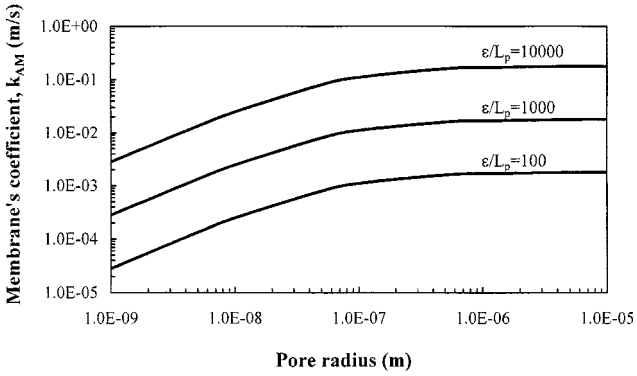

Figure 5. Effect of pore radius on membrane's coefficient, k_{AM}, evaluated for different effective porosity.

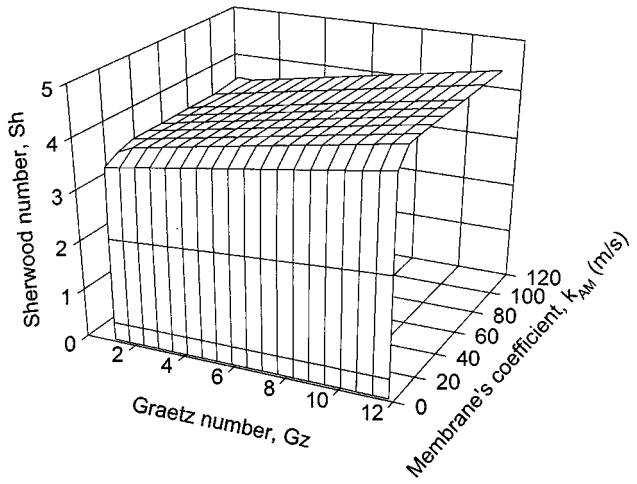

Figure 6. Sherwood number vs. Graetz number for different values of k_{AM}, simulation results.

values of k_{AM} obtained from these two independent analyses are in the same order of magnitude. It thus follows that the gas permeation method may be a simple and useful technique for employing various permanent gases in the first estimation of the membrane's coefficients.

Effect of gas velocity

The effect of the gas velocity on the overall mass-transfer coefficients was first studied theoretically. The values of the overall mass-transfer coefficients were calculated using the mean logarithmic driving force (Skelland, 1974b). Figure 6 shows the effects of the Graetz number, *Gz* (the gas velocity), and the membrane's coefficient, k_{AM}, on the Sherwood number, *Sh* (the overall mass-transfer coefficient, K_{AG}), plotted in three dimensions. As can be seen, the overall mass-transfer coefficient is generally independent of the gas velocity when the membrane's coefficient, k_{AM}, is small. At a negligible membrane resistance, that is, $k_{AM} = 100$ m/s, the overall mass-transfer coefficient varies with gas velocity (Sherwood numbers obtained are between 3.69 and 4.28, corresponding to the K_{AG} values between 0.117 and 0.140 m/s at Graetz number less than 9).

Figure 7 illustrates the experimental effect of gas velocities in hollow-fiber lumens on the overall mass-transfer coefficients for the nine modules studied. We can see that the overall mass-transfer coefficients are independent of the gas velocity for almost all the modules studied, except module 9 where the dependence of the overall mass-transfer coefficient on the gas velocity can be seen. Further analysis of the overall mass-transfer coefficients for these nine modules indicates that only the k_{AG} values of module 9 (between 0.036 and 0.051 m/s) are of the same magnitude as the mass-transfer coefficient in the gas phase, while the rest are all considerably smaller. Therefore, membrane resistance still dominates the mass-transfer process for these modules, except for the module 9, where both the gas film resistance ($1/k_{AG}$) and membrane resistance ($1/k_{AM}$) are important.

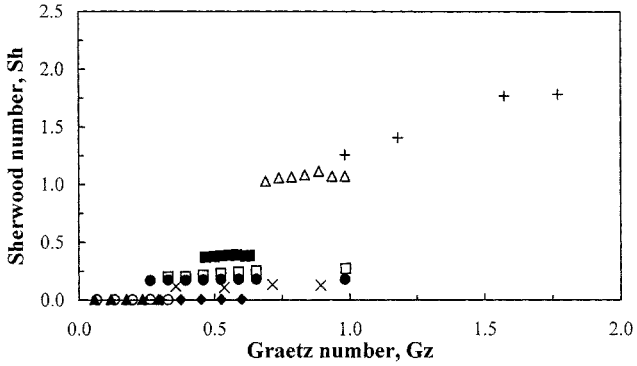

Figure 7. Sherwood number vs. Graetz number for the different membrane modules, experimental results from membrane modules: ○: 1; ◆: 2; ▲: 3; ×: 4; ●: 5; □: 6; ■: 7; △: 8; +: 9.

Comparison of k_{AM} with values in the literature

The experimental values of k_{AM} obtained in this study are also compared in Table 3 with those published values obtained from symmetric polypropylene membranes and an asymmetric polysulfone membrane. As can be seen, the k_{AM} values of the prepared PVDF asymmetric hollow-fiber membranes are considerably greater than those obtained from the symmetric polypropylene membranes. Comparison between the asymmetric polysulfone membrane and the PVDF membranes studied indicate that their k_{AM} values are comparable when the coagulation conditions, that is, water used as both internal and external coagulants, employed in preparing the PVDF membranes are the same as those used in preparing the polysulfone membrane. When the internal coagulant is changed to ethanol, the k_{AM} value is considerably larger, which therefore suggests that asymmetric membranes with a much higher k_{AM} value, could be prepared for H_2S transfer. To achieve this, the porosity of the membrane in the skin layer must be high (achieved by adding PVP), and the resistance in the membrane substrate must be low (achieved by using ethanol or an ethanol/water mixture as a coagulant). Furthermore, in order to prevent the membrane from getting wet, the mean pore size of the membrane must also be small, and the PVP additive must be thoroughly washed out of the prepared membrane.

Conclusions

Tailor-made asymmetric PVDF hollow-fiber membranes and their membrane modules were used to remove soluble

Table 3. Comparison of k_{AM} Values

	Membranes	k_{AM} Values, m/s
Zhang and Cussler (1985b)	Symmetric polypropylene (Microporous)	0.0073 (exp.)
Kreulen et al. (1992)	Symmetric polypropylene (Microporous)	0.019 (calculated)
Li et al. (1998)	Asymmetric polysulfone (Microporous)	0.0125–0.025 (exp.)
This study	Asymmetric PVDF (Microporous)	0.012–0.072 (exp.)

gas, such as H_2S, from waste gas streams. The membranes with different morphological structures were prepared using a phase-inversion process, and were characterized by using SEM and gas permeation techniques. Results from the SEM study reveal that the skin location is largely dependent on the coagulation medium. The addition of a substantial amount of ethanol to the coagulation medium would greatly affect the formation of the skin. Experimental results obtained from the nine different membrane modules developed also indicate that a PVDF membrane with much reduced membrane resistance could be prepared by properly selecting the internal coagulation and using PVP as an additive in its polymer-forming solution. The membrane's coefficient, k_{AM}, evaluated from the structure parameters, such as the effective surface porosity and mean radius, agreed well with the experimental data obtained from absorption experiments. Comparison of the membrane's coefficient, k_{AM}, of the asymmetric PVDF membranes with that of the symmetric polypropylene membranes reveals that the k_{AM} values for the PVDF membranes are considerably higher, especially for module 9. The overall mass-transer coefficient, K_{AG}, obtained from module 9 is in the 0.036 to 0.051-m/s range, which is almost the same magnitude as the values measured in the conventional gas absorbers (0.01–0.1 m/s; Westerterp et al., 1984).

Acknowledgments

The authors gratefully acknowledge the research funding (GR6456) provided by the Wheelabrator Water Technology (S) Ltd., Singapore. A research scholarship provided by the National University of Singapore to one of the authors (J. F. K.) is also gratefully acknowledged.

Notation

C_a = concentration of H_2S, mol/m^3
C_{ai} = interfacial concentration of H_2S, mol/m^3
D_a = diffusivity of H_2S, m^2/s
k_{AG} = gas film mass-transfer coefficient, m/s
K_{AG} = overall mass-transfer coefficient of H_2S, m/s
K_0 = a constant defined in Eq. 1
L_p = effective pore length, m
M = molecular weight
P_0 = a constant defined in Eq. 1
$\bar{p}$ = mean pressure, Pa
Q_{AG} = feed-gas flow rate, m^3/s
r = radial coordinate, m
R = inner diameter of the fiber, m
R_0 = outer diameter of the fiber, m
T = absolute temperature, K
U = gas velocity in fiber, m/s
$X_{a,\text{out}}$ = ratio of product concentration and feed concentration of H_2S, $C_{a,\text{out}}/C_{af}$
U_m = average gas velocity in fiber, $(= Q_{AG}/n\pi R^2)$ m/s
Z = module length, m
z = axial coordinate, m
μ = viscosity of gas, pa·s

Subscripts

i = gas species

Literature Cited

Ahmed, T., and M. J. Semmens, "Use of Sealed End Hollow Fibers for Bubbleless Membrane Aeration: Experimental Studies," *J. Memb. Sci.*, **69**, 1 (1992).
Cooney, D., and C. Jackson, "Gas Absorption in a Hollow Fiber Device," *Chem. Eng. Commun.*, **79**, 153 (1989).
Costello, M. J., A. G. Fane, P. A. Hogan, and R. W. Schofield, "The Effect of Shell Side Hydrodynamics of the Performance of Hollow Fiber Modules," *J. Memb. Sci.*, **80**, 1 (1993).
Danckwerts, P. V., *Gas Liquid Reactions*, McGraw-Hill, New York (1970).
Deshmukh, S. P., and K. Li, "Effect of Ethanol Composition in Water Coagulation Bath on Morphology of PVDF Hollow Fiber Membranes," *J. Memb. Sci.*, **150**, 75 (1998).
Finlayson, B. A., "Packed Bed Reactor Analysis by Orthogonal Collocation," *Chem. Eng. Sci.*, **26**, 1081 (1971).
Karoor, S., and K. K. Sirkar, "Gas Absorption Studies in Microporous Hollow Fiber Membrane Modules," *Ind. Eng. Chem. Res.*, **32**, 674 (1993).
Kreulen, H., C. A. Smolders, G. F. Versteeg, and W. P. M. van Swaaij, "Determination of Mass Transfer Rates in Wetted and Non-Wetted Microporous Membranes," *Chem. Eng. Sci.*, **48**, 2093 (1993a).
Kreulen, H., C. A. Smolders, G. F. Versteeg, and W. P. M. van Swaaij, "Microporous Hollow Fiber Membrane Modules as Gas-Liquid Contactors: 1. Physical Mass Transfer Processes, A Specific Application: Mass Transfer in Highly Viscous Liquids," *J. Memb. Sci.*, **78**, 197 (1993b).
Kreulen, H., C. A. Smolders, G. F. Versteeg, and W. P. M. van Swaaij, "Microporous Hollow Fiber Membrane Modules as Gas-Liquid Contactors: 2. Mass Transfer with Chemical Reaction," *J. Memb. Sci.*, **78**, 217 (1993c).
Li, K., M. S. L. Tai, and W. K. Teo, "Design of a CO_2 Scrubber for Self-Contained Breathing Systems Using a Microporous Membrane," *J. Memb. Sci.*, **86**, 119 (1994).
Li, K., D. Wang, C. C. Koe, and W. K. Teo, "Use of Asymmetric Hollow Fiber Membrane Modules for Elimination of H_2S from Gas Streams via a Membrane Absorption Method," *Chem. Eng. Sci.*, **53**, 1111 (1998).
Malek, A., K. Li, and W. K. Teo, "Modelling of Micromorous Hollow Fiber Membrane Modules Operated Under Partially Wetted Conditions," *Ind. Eng. Chem. Res.*, **36**, 784 (1997).
Munari, S., A. Bottino, G. Camera-Roda, and G. Capannelli, "Preparation of Ultrafiltration Membranes. State of the Art," *Desalination*, **77**, 85 (1990).
Present, R. D., *Kinetic Theory of Gases*, McGraw-Hill, New York (1958).
Shih, H. C., Y. S. Yeh, and H. Yasuda, "Morphology of Microporous Poly(vinylidene Fluoride) Membranes Studied by Gas Permeation and Scanning Microscopy," *J. Memb. Sci.*, **50**, 299 (1990).
Skelland, A. H. P., *Diffusional Mass Transfer*, Wiley, New York, p. 154 (1974a).
Skelland, A. H. P., *Diffusional Mass Transfer*, Wiley, New York, p. 157 (1974b).
Wang, D., K. Li, and W. K. Teo, "Effect of Temperature and Pressure on Gas Permselection Properties in Asymmetric Membranes," *J. Memb. Sci.*, **105**, 89 (1995).
Westerterp, K. R., W. P. M. van Swaaij, and A. A. C. M. Beenackers, *Chemical Reactor Design and Operation*, Wiley, New York (1984).
Yang, M., and E. L. Cussler, "Designing Hollow-Fiber Contactors," *AIChE J.*, **32**, 1910 (1986).
Zhang, Q., and E. L. Cussler, "Microporous Hollow Fibers for Gas Absorption: I. Mass Transfer in the Liquid," *J. Memb. Sci.*, **23**, 321 (1985a).
Zhang, Q., and E. L. Cussler, "Microporous Hollow Fibers for Gas Absorption: II. Mass Transfer Across the Membrane," *J. Memb. Sci.*, **23**, 333 (1985b).

Appendix

The permeation of gas through asymmetric membranes is mainly determined by the skin layer (Shih et al., 1990). The total rate of gas permeation through the asymmetric membranes can be expressed in a general nonmechanical flux equation in terms of Poiseuille flow and Knudsen flow in the porous medium as follow:

$$N_{t,i} = P_{v,i} A_p \frac{\Delta p}{L_p} + P_{k,i} A_p \frac{\Delta p}{L_p}, \qquad \text{(A1)}$$

where $N_{t,i}$ is the total permeation flow rate (mol/s); A_p is the porous area on the membrane surface (m^2); L_p is the effective pore length (m); P_v and P_k are gas transport permeability coefficients according to Poiseuille flow and Knudsen flow mechanisms (mol·m/m^2·Pa·s), respectively; Δp is the pressure difference across the membrane (Pa); and subscript i refers to the gas species concerned. Equation A1 is based on the following assumptions: the pores in the skin layer are approximately the same as the cylindrical pores, which have modal pore radius, r, and effective length, L_p.

Because the skin-layer thickness of the asymmetric membranes is usually an unknown value and cannot be determined using available methods, the total gas permeation rate through the asymmetric membranes is usually expressed as

$$N_{t,i} = J_i A_t \Delta p, \tag{A2}$$

where J_i is the gas permeability (mol/m^2·Pa·s), and A_t is the total membrane permeation area (m^2). The surface porosity of the skin layer is defined as

$$\epsilon = \frac{A_p}{A_t}. \tag{A3}$$

Substituting Eqs. A2 and A3 into Eq. A1 and rearranging, the following equation is obtained:

$$J_i = P_{v,i}\frac{\epsilon}{L_p} + P_{k,i}\frac{\epsilon}{L_p} \tag{A4}$$

When a gas is transferred by Poiseuille flow through a long straight capillary tube with a pore radius of r, the molar flux is expressed as (Present, 1958)

$$F_v = \frac{r^2}{8\mu RT}\bar{p}\frac{\Delta p}{L_p}, \tag{A5}$$

where F_v is molar flux (mol/m^2·s); r is radius of the capillary tube (m); μ is the viscosity of gas (Pa·s); R is the gas constant (8.3174 m^3·Pa/mol·K); $\bar{p}$ is the mean pressure (Pa); and T is absolute temperature (K). For the purpose of determining the permeability coefficient by Poiseuille flow, Eq. A5 is rewritten as

$$\frac{F_v L_p}{\Delta P} = P_{v,i} = \frac{1}{8\mu}\frac{r^2}{RT}\bar{p}. \tag{A6}$$

When using Knudsen flow to transfer a gas through a long capillary tube with the radius of r, its molar flux is expressed as (Present, 1958)

$$F_k = \frac{2}{3}\left(\frac{8RT}{\pi M}\right)^{0.5}\frac{1}{RT}\frac{\Delta p}{L_p}, \tag{A7}$$

where F_k is the gas molar flux (mol/m^2·s), and M is the molecular weight (g/mol). In order to determine the Knudsen permeability coefficient, Eq. A7 is rewritten in the following form:

$$\frac{F_k L_p}{\Delta p} = P_{k,i} = \frac{2}{3}\left(\frac{8RT}{\pi M}\right)^{0.5}\frac{r}{RT}. \tag{A8}$$

Substituting Eqs. A6 and A8 into Eq. A4, we get Eq. 1.

Manuscript received Dec. 29, 1998, and revision received Apr. 13, 1999.